Structure of AMP-PNP-bound BtuCD and mechanism of ATP-powered vitamin B12 transport by BtuCD-F

Originally published in:
Nature Structural & Molecular Biology 21(12), https://doi.org/10.1038/nsmb.2918

Structure of AMPPNP-bound BtuCD and reaction mechanism of ATP-powered vitamin B12 transport by BtuCD-F

Vladimir M. Korkhov[1,2], Samantha A. Mireku[1], Dmitry Veprintsev[2] and Kaspar P. Locher[1*]

Author affiliations:

[1] Institute of Molecular Biology and Biophysics, ETH Zurich, Otto-Stern-Weg 5, 8046, Zurich, Switzerland

[2] Laboratory of Biomolecular Research, Paul Scherrer Institute, Villigen, Switzerland

* Corresponding author: kaspar.locher@mol.biol.ethz.ch

The reaction mechanism of BtuCD-F-catalyzed vitamin B12 transport into Escherichia coli is currently unclear. Here we present the structure of the last missing state in the form of AMPPNP-bound BtuCD, trapped using a disulfide cross-link. Our structural and biochemical data allow a consistent mechanism to be formulated, rationalizing the roles of substrate, ATP, and binding protein.

ABC transporters catalyze ATP hydrolysis-driven transport of diverse substrates across biological membranes[1]. Type II ABC importers, present only in prokaryotes, facilitate the uptake of metal chelates including siderophores, heme and vitamin B12[2], all essential micro-nutrients whose uptake is critical for the survival or virulence of various pathogens. After the first structure of BtuCD was determined[3], divergent mechanistic proposals have been made, but no consistent mechanism could reconcile biochemical and structural data of type II ABC importers. We now report the structure of AMPPNP-bound BtuCD in the absence of BtuF, which likely represents the most populated state of BtuCD in live cells and thus is a crucial intermediate in the transport cycle.

To crystallize AMMPNP-bound BtuCD, two previously exploited mutations in the BtuD subunit (E159Q and N162C) allowed nucleotide-bound BtuD to be trapped in a closed sandwich conformation and the residual ATPase rate to be dramatically reduced[4]. Anisotropic X-ray data (2.8-3.7Å) was collected from three crystals, and the structure was solved by molecular replacement (Supplementary Table 1). Clear density for all critical features was visible in the electron density maps (Supplementary Fig. 1). The structure of AMPPNP-bound $BtuCD_{EQNC}$ (Fig. 1) revealed the closed sandwich dimer of the BtuD subunits, with two AMPPNP/Mg^{2+} pairs bound. The coupling helices of BtuC are ~9.4Å closer in $BtuCD_{EQNC}$ compared to the apo-structures of BtuCD and BtuCD-F, and the cytoplasmic side of the transport cavity is sealed by cytoplasmic gate II. However, unlike the occluded conformation of AMPPNP-bound $BtuCD_{EQNC}$-F, $BtuCD_{EQNC}$ adopts an outward-open conformation reminiscent of apo-BtuCD. With respect to the gate positions, the structure of $BtuCD_{EQNC}$ is therefore a hybrid between apo-BtuCD (similar at periplasmic side) and $BtuCD_{EQNC}$ -F (similar at cytoplasmic side). Given that the cytoplasmic concentration of ATP in live cells is in the millimolar range, visualizing the ATP-bound state of BtuCD was essential to formulating a complete B12 transport mechanism. Multiple observations support the notion that the observed structure

accurately reflects ATP-bound, wild type BtuCD. First, the observed BtuD dimer has a similar conformation as other ATP-bound NBD structures. Second, the closing of the cytoplasmic gate II and the simultaneous opening of cytoplasmic gate I (and TM10) were observed by EPR spectroscopy of BtuCD in the presence of ATP or AMPPNP in detergent and in lipid bilayers[5]. Third, EPR spectroscopy revealed very minor changes in the conformation of the periplasmic gate upon addition of nucleotide to BtuCD[6].

To further validate the physiological relevance of our findings, we confirmed that $BtuCD_{EQNC}$ could interact with BtuF similar to wild type transporter by performing *in vitro* binding studies using fluorescein-labeled BtuF ("$BtuF_{fluo}$", Supplementary Fig. 2). In microscale thermophoresis (MST) experiments (an equilibrium binding technique), both BtuCD and $BtuCD_{EQNC}$ showed similar affinities for $BtuF_{fluo}$, with K_d values in the nanomolar range. The presence of AMPPNP did not significantly alter the apparent affinities (Supplementary Fig. 3). Notably, using sedimentation velocity analytical ultracentrifugation (a non-equilibrium technique), the addition of AMPPNP appeared to reduce the strength of the BtuCD-BtuF interaction.

Because the interaction of BtuF with BtuCD may be influenced by the lipidic environment, we studied the binding of $BtuF_{fluo}$ to proteoliposome-reconstituted BtuCD (Supplementary Fig. 4) Compared to empty proteoliposomes, entrapped AMPPNP caused a slight increase of liposome-bound $BtuF_{fluo}$, whereas ATP (supported by an ATP regeneration system) caused a ~2-fold increase, indicating a higher apparent affinity. $BtuF_{fluo}$ could readily be displaced by unlabeled BtuF, and despite a molar excess of BtuCD, only a fraction of total $BtuF_{fluo}$ was bound. In the presence of vitamin B12, the fraction of bound $BtuF_{fluo}$ was reduced, but $BtuF_{fluo}$ binding was observed even in the presence of a 100-fold excess of vitamin B12 over binding protein (with ATP present in the proteoliposome lumen). We also studied the binding of $BtuF_{fluo}$ to nanodisc-reconstituted BtuCD by size exclusion chromatography (Supplementary Fig. 5). Incubation of transporter/$BtuF_{fluo}$ mixtures with ATP caused a sizeable increase in complex formation compared to that in the absence of nucleotide, demonstrating a higher apparent affinity. Moreover, our MST experiments with $BtuF_{fluo}$ and nanodisc-reconstituted BtuCD suggested that the BtuCD-$BtuF_{fluo}$ interaction was in the micromolar range (almost 3 orders of magnitude higher than in detergent and regardless of the presence of ATP; not shown). We conclude from our binding studies

that BtuF does not require an ATP “trigger” to be released from BtuCD. Rather, ATP promotes docking of B12-loaded BtuF and thus accelerates transport.

The complete mechanism of BtuCD-catalyzed B12 transport is shown in Figure 2; this mechanism may serve as a model for other type II ABC importers. A productive cycle of B12 transport starts with ATP-bound BtuCD (state 1), which is based on the AMPPNP-bound $BtuCD_{EQNC}$ structure reported here: ATP binding triggers closure of the BtuD dimer, resulting in the opening of cytoplasmic gate I and simultaneous closing of cytoplasmic gate II. Subsequent docking of B12-bound BtuF to BtuCD leads to state 2 (PDB ID: 4FI3), wherein B12 can be trapped in a central, low-affinity cavity. State 2 is an occluded conformation. To reach state 3, hydrolysis of ATP and release of P_i/ADP disrupts the closed sandwich dimer conformation of the BtuD subunits. The coupling helices and cytoplasmic gates II are pulled open, leading to the formation of a transient, inward-facing conformation, allowing B12 release into the cytoplasm. This state is visualized by the structure of Hi1470/71, a homologue of BtuCD[4] (PDB ID: 2NQ2), but no direct structural information is available for BtuCD. The inward-facing conformation is probably short-lived, relaxing into asymmetric state 4 as soon as B12 is released. The observed asymmetry in the cytoplasmic gates I in state 4 is not connected to that of BtuF, based on structural evidence[7,8] (PDB ID: 2QI9 and 4DBL). State 4 is very stable in detergent solution and does not contain any cavity of sufficient size to harbor B12. This state may prevent the back-reaction or non-specific transport of solutes through the translocation pathway. From state 4, there are two possible ways (Fig. 2), dependent on the local nucleotide concentration in the vicinity of BtuCD in the *E. coli* inner membrane. State 5 can be reached by dissociation of BtuF and re-arrangement of the cytoplasmic gates I to reach a symmetric, outward-facing conformation. Given the high intra-cellular levels of ATP, state 5 probably rapidly converts to state 1, with the cytoplasmic gates I and II switching positions. *In vitro*, states 5 and "2-like" are readily formed, and it cannot be excluded that they also occur *in vivo*[3,9]. The transitions into these states, specifically between states 4 and 2-like and states 1 and 5, invoke futile ATPase activity (ATP hydrolysis without transport), an inherent inefficiency of the transporter that is consistent with published observations[10]. Futile ATP hydrolysis makes it impossible to accurately determine the stoichiometry of ATP hydrolysis to substrate transport. For one well-coupled system, the OpuA system from *Lactococcus lactis*, a stoichiometry of two ATP hydrolysed per transported substrate was determined[11]. We assume that

BtuCD, having two symmetrical and canonical ATPase sites, also hydrolyzes two ATP molecules during each productive transport cycle.

BtuCD is part of a high-affinity uptake process in *E. coli*. The high affinity (nanomolar K_d) and specificity for B12 in the transport step across the inner (plasma) membrane can be exclusively attributed to the binding protein BtuF. Upon docking to BtuCD, its high-affinity pocket for B12 is both distorted and occupied by residues of the periplasmic gate of BtuC. The BtuF-BtuCD interaction is strengthened by ATP binding, but the structural basis of this subtle regulation is currently not understood. The weaker affinity of interaction between BtuF and BtuCD in lipid bilayer is reminiscent of other ABC transporter systems including the maltose transporter (type I ABC transporter[12]), in which the periplasmic maltose binding protein stimulates the ATPase activity of the membrane-embedded counterpart, $MalFGK_2$, when present at micromolar concentrations[13]. Low affinity interactions prevent clogging of the transport machinery and ensure efficient turnover. The mechanism of type II ABC importer function presented here complies with these requirements for effective substrate translocation.

METHODS

Protein expression and purification. BtuCD and $BtuCD_{EQNC}$ complexes were purified and oxidized by $CuCl_2$ (for $BtuCD_{EQNC}$) as described previously[4], in a final buffer of the following composition: 20 mM Tris (pH7.5), 500 mM NaCl, 0.5 mM EDTA, 0.1% LDAO. For crystallization, 3C protease cleavage step was performed prior to oxidation.

Expression and purification of BtuF and $BtuF_{Q145C}$ followed established procedures[8].

Membrane scaffold protein for nanodisc reconstitution, MSP1-E3D1[14], was expressed and purified as described previously[14].

Proteoliposome reconstitution. Procedure for reconstitution of BtuCD into proteoliposomes followed that described previously[4].

Nanodisc reconstitution. Purified BtuCD complex in LDAO was mixed with purified MSP1-E3D1 and lipids (*E. coli* polar lipids and phosphatidylcholine, 3:1, solubilized in 4% Triton X-100), at final concentrations of 12 μM, 72 μM and 2.5 mM; the concentration of lipid mixture was estimated based on molecular weights of the major lipid components. Concentration of Triton X-100 was adjusted to 1%. Following 30 min incubation at room temperature, the detergent was removed by BioBeads stepwise overnight, using 0.1-0.5g Biobeads/1 ml mixture. After detergent removal the samples were further purified by Ni-NTA using 10xHis tag present in BtuC N-terminus and gel filtration.

Centrifugation-based BtuF binding assays. ATP regeneration system was introduced into the lumen of the proteoliposomes by four freeze-thaw cycles, followed by sonication. BtuF binding was initiated by adding fluorescein-labeled BtuF to the BtuCD proteoliposomes and 10 min incubation at room temperature (22 °C), in 20 mM Tris (pH 7.5), 200 mM NaCl, 0.5 mM EDTA, 5 mM $MgCl_2$, 1% BSA. After 10 min centrifugation at 4 °C using a bench-top centrifuge (16900g), supernatants were carefully removed, leaving the proteoliposome pellets intact. Pellets were resuspended in 0.5% Triton X-100 and fluorescence associated with the proteoliposomes was measured using a fluorescence plate reader (ex. 485/20 nm, em. 528/20 nm, sensitivity 50-75). For experiments with vitamin B12, pellets were resuspended in 0.5% SDS to avoid fluorescein quenching by vitamin B12 associated with BtuF.

Analytical ultracentrifugation. Analytical centrifugation was performed using ProteomeLab XL-I analytical centrifuge (Beckman) equipped with fluorescence detection system (AVIV Biomedical). Sedimentation velocity experiments were performed using $BtuF_{fluo}$ and BtuCD or $BtuCD_{EQNC}$ in 50 mM Tris (pH 7.5), 500 mM NaCl, 0.5 mM EDTA, 5 mM $MgCl_2$ ± 1 mM AMPPNP, at 10 °C, at 50000 rpm, as described previously[15]. Buffer density and viscosity were calculated using the SEDNTERP software. Sedimentation coefficient traces were calculated using the SEDFIT software[16].

Microscale thermophoresis. Microscale thermophoresis was performed using Monolith NT.115 (NanoTemper Technologies), following the manufacturer's instructions. The results were analysed using NanoTemper software and GraphPad Prism 5 to determine K_d values. GraphPad Prism 5 was used to plot the data and perform statistical analysis (one-way ANOVA).

Protein crystallization and data collection. Purified, tag-free, cross-linked $BtuCD_{EQNC}$ at 16-20 mg/ml in 20 mM Tris, 500 mM NaCl, 0.5 mM EDTA, 5 mM $MgCl_2$, 2 mM AMPPNP, was mixed with 1:1 with reservoir solution containing 100 mM ADA (pH 6.9), 1.2 M NaCl, 14-18% PEG2000MME and crystallized by vapour diffusion in sitting drops. Crystals grew at 10 °C and were cryo-protected by step-wise addition of a harvesting solution containing increasing concentrations of PEG2000MME to 30-32% before cooling in liquid nitrogen.

Crystallographic data processing and model building. Data processing was performed using HKL2000[17], ellipsoidal truncation and anisotropic scaling was performed as described[18]. The structure was solved by molecular replacement, model building was performed using Coot[19], refinement using Phenix[20] (Supplementary Table 1).

FIGURE LEGENDS

Figure 1: Structure of AMPPNP-bound $BtuCD_{EQNC}$ (a) Side view. BtuC subunits are colored marine and blue, BtuD subunits forest and pale green. **(b)** Comparison of apo-BtuCD ("BtuCD", pdb ID 1L7V) and $BtuCD_{EQNC}$/AMPPNP ("EQNC/AMPPNP") illustrating movement of coupling helices (indicated by arrows) but similarly open periplasmic gates. **(c,d)** View of apo-BtuCD (**c**) and $BtuCD_{EQNC}$/AMPPNP (**d**) from the cytoplasmic side of the membrane. Atoms of residues forming cytoplasmic gate I (residues 141-143) and gate II (residues 83-85) are shown as spheres and colored as indicated.

Figure 2: Mechanism of BtuCD-F-catalyzed B12 transport. Grey cylinder cartoons illustrate structures of BtuCD, BtuF, or BtuCD-F, circled numbers indicate states as discussed in text. Yellow ball-and-sticks represent nucleotides, red ball-and-sticks depict cobalamin. Thick blue lines depict transmembrane helices 5 in each BtuC subunit, forming the periplasmic gates and the cytoplasmic gates I. Purple brackets depict the cytoplasmic gates II in each BtuC subunit.

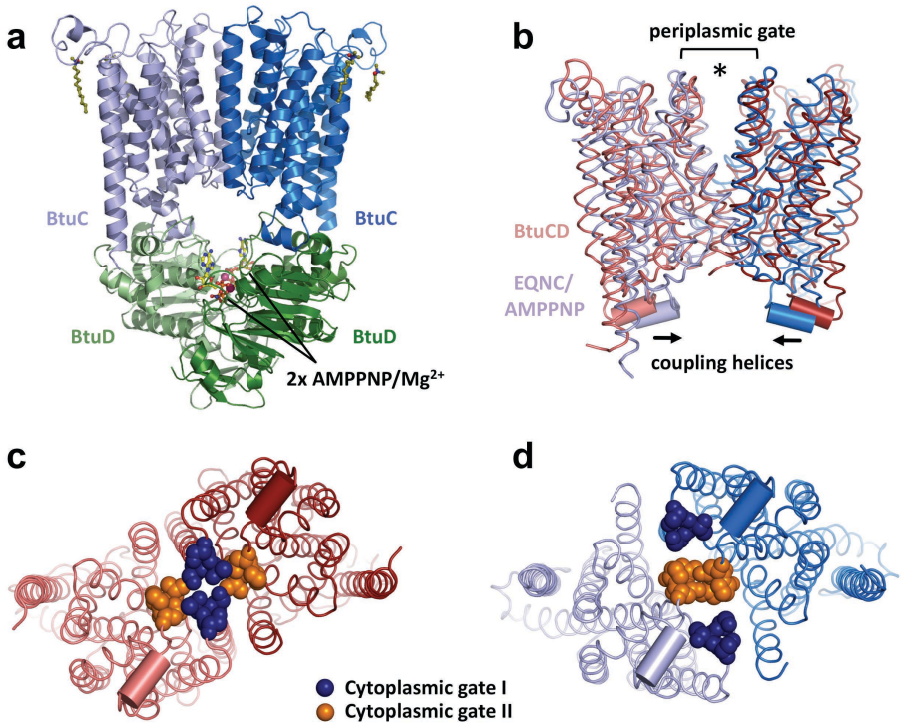

Figure 1: Structure of AMPPNP-bound BtuCD$_{EQNC}$ (a) Side view. BtuC subunits are colored marine and blue, BtuD subunits forest and pale green. **(b)** Comparison of apo-BtuCD ("BtuCD", pdb ID 1L7V) and BtuCD$_{EQNC}$/AMPPNP ("EQNC/AMPPNP") illustrating movement of coupling helices (indicated by arrows) but similarly open periplasmic gates. **(c,d)** View of apo-BtuCD (**c**) and BtuCD$_{EQNC}$/AMPPNP (**d**) from the cytoplasmic side of the membrane. Atoms of residues forming cytoplasmic gate I (residues 141-143) and gate II (residues 83-85) are shown as spheres and colored as indicated.

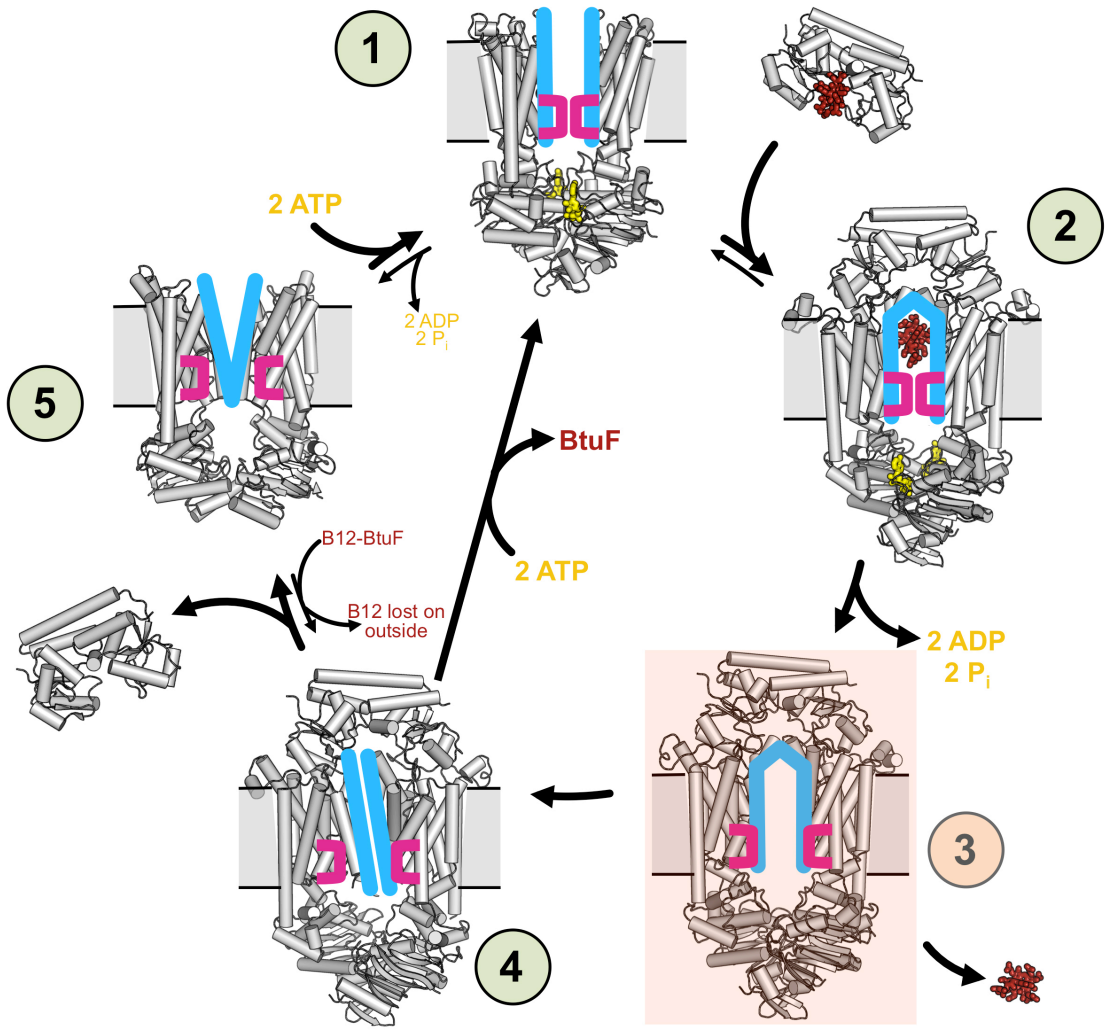

Figure 2: Mechanism of BtuCD-F-catalyzed B12 transport. Grey cylinder cartoons illustrate structures of BtuCD, BtuF, or BtuCD-F, circled numbers indicate states as discussed in text. Yellow ball-and-sticks represent nucleotides, red ball-and-sticks depict cobalamin. Thick blue lines depict transmembrane helices 5 in each BtuC subunit, forming the periplasmic gates and the cytoplasmic gates I. Purple brackets depict the cytoplasmic gates II in each BtuC subunit.

REFERENCES

1. Rees, D.C., Johnson, E. & Lewinson, O. *Nat Rev Mol Cell Biol* **10**, 218-27 (2009).
2. Klein, J.S. & Lewinson, O. *Metallomics* **3**, 1098-108 (2011).
3. Locher, K.P., Lee, A.T. & Rees, D.C. *Science* **296**, 1091-8 (2002).
4. Korkhov, V.M., Mireku, S.A. & Locher, K.P. *Nature* **490**, 367-72 (2012).
5. Joseph, B., Korkhov, V.M., Yulikov, M., Jeschke, G. & Bordignon, E. *J Biol Chem* (2013).
6. Joseph, B., Jeschke, G., Goetz, B.A., Locher, K.P. & Bordignon, E. *J Biol Chem* **286**, 41008-17 (2011).
7. Hvorup, R.N. et al. *Science* **317**, 1387-90 (2007).
8. Korkhov, V.M., Mireku, S.A., Hvorup, R.N. & Locher, K.P. *FEBS Lett* **586**, 972-6 (2012).
9. Woo, J.S., Zeltina, A., Goetz, B.A. & Locher, K.P. *Nat Struct Mol Biol* **19**, 1310-5 (2012).
10. Borths, E.L., Poolman, B., Hvorup, R.N., Locher, K.P. & Rees, D.C. *Biochemistry* **44**, 16301-9 (2005).
11. Patzlaff, J.S., van der Heide, T. & Poolman, B. *J Biol Chem* **278**, 29546-51 (2003).
12. Chen, J. *Curr Opin Struct Biol* **23**, 492-8 (2013).
13. Gould, A.D., Telmer, P.G. & Shilton, B.H. *Biochemistry* **48**, 8051-61 (2009).
14. Ritchie, T.K. et al. *Methods Enzymol* **464**, 211-31 (2009).
15. Brandt, T., Petrovich, M., Joerger, A.C. & Veprintsev, D.B. *BMC Genomics* **10**, 628 (2009).
16. Schuck, P., Perugini, M.A., Gonzales, N.R., Howlett, G.J. & Schubert, D. *Biophys J* **82**, 1096-111 (2002).
17. Otwinowski, Z. & Minor, W. *Macromolecular Crystallography, Pt A* **276**, 307-326 (1997).
18. Strong, M. et al. *Proc Natl Acad Sci U S A* **103**, 8060-5 (2006).
19. Emsley, P., Lohkamp, B., Scott, W.G. & Cowtan, K. *Acta Crystallogr D Biol Crystallogr* **66**, 486-501 (2010).
20. Adams, P.D. et al. *Acta Crystallogr D Biol Crystallogr* **66**, 213-21 (2010).

Structure of AMPPNP-bound BtuCD and reaction mechanism of ATP-powered vitamin B12 transport by BtuCD-F

Vladimir M. Korkhov[1,2], Samantha A. Mireku[1], Dmitry Veprintsev[2] and Kaspar P. Locher[1*]

Author affiliations:

[1] Institute of Molecular Biology and Biophysics, ETH Zurich, Otto-Stern-Weg 5, 8046, Zurich, Switzerland

[2] Laboratory of Biomolecular Research, Paul Scherrer Institute, Villigen, Switzerland

* Corresponding author: kaspar.locher@mol.biol.ethz.ch

ABSTRACT

ATP-dependent uptake of essential metal-chelate micronutrients into bacteria is catalyzed by type II ABC transporters. A well-studied example is BtuCD-F, which catalyzes vitamin B12 transport, but whose mechanism of a full reaction cycle remained unclear. Here we present the structure of AMPPNP-bound BtuCD trapped by disulfide cross-linking. We find a hybrid conformation of the transmembrane BtuC subunits, with an outward-exposed central cavity and cytoplasmic gate II replacing gate I in sealing the transport towards the cytoplasm. Unexpectedly, *in vitro* binding studies revealed that ATP enhances the affinity of BtuCD for BtuF when the transporter is reconstituted in proteoliposomes or nanodiscs. In contrast, the affinity of detergent -embedded BtuCD for BtuF is three orders of magnitude larger and insensitive to ATP. Our data allow us to formulate a consistent mechanism of BtuCD that rationalizes the roles of substrate, ATP, and binding protein.

INTRODUCTION

ABC transporters catalyze diverse substrate transport reactions across biological membranes in an ATP binding- and hydrolysis-dependent manner[1,2]. A sub-family of ABC transporters, the "type II ABC importers", are present only in prokaryotic genomes and facilitate the uptake of metal chelates including siderophores, heme and vitamin B12[3]. These substrates are essential micro-nutrients for bacteria and their uptake is critical for the survival or virulence of various pathogens. The vitamin B12 transporter of the Gram-negative bacterium *Escherichia coli*, BtuCD-F, is a well-studied type II ABC transporter. The transport moiety BtuCD consists of two nucleotide binding subunits (BtuD), each attached by non-covalent interactions to a transmembrane subunit (BtuC). After vitamin B12 is transported across the outer membrane into the periplasm (in a TonB-dependent process mediated by outer membrane transporter, BtuB[4]) it is scavenged by the high affinity periplasmic binding protein, BtuF and delivered to BtuCD in the *E. coli* inner membrane. Binding and hydrolysis of ATP molecules by the dimer of BtuD subunits induces conformational changes in the BtuC subunits, leading to movement of vitamin B12 into the cytoplasm of *E. coli* cells[5,6].

Since the first structure of BtuCD was determined over a decade ago[6], distinct mechanistic proposals of BtuCD (and other type II ABC importer) function have been proposed and, as a consequence, no consistent and widely accepted mechanism reconciling the available biochemical and structural data has emerged. In particular, the precise role of ATP binding and hydrolysis and the release of BtuF after a completed transport cycle are unclear. Our previous work demonstrated that binding of a non-hydrolysable ATP analogue, AMPPNP, promotes transport of vitamin B12 into an occluded cavity half-way through the membrane[7]. In contrast, another study suggested that the function of ATP binding may be to destabilize the full BtuCD-F complex, promoting BtuF dissociation and thus preparing the protein for the next transport cycle[8].

Here, we provide structural and biochemical data that allow us to formulate a complete B12 transport cycle. By determining a critically important structure, that of AMPPNP-bound BtuCD in the absence of BtuF, we demonstrate that nucleotide binding to BtuCD causes rearrangements of the cytoplasmic gating regions, while maintaining an outward-open conformation. The observed conformation likely represents the most highly populated state of BtuCD in live cells and a crucial intermediate in a productive B12 transport cycle, during which ATP binding appears to prime BtuCD for enhancing the binding of B12-loaded BtuF. By combining biochemical and biophysical techniques, we demonstrate that BtuF can readily dissociate from transporter under physiologically relevant conditions in the lipid bilayer, and that the presence of ATP/Mg^{2+} enhances BtuF-BtuCD interaction rather than promoting complex dissociation. Combining our new structure with the previously published apo-structures of BtuCD and BtuCD-F and that of AMPPNP-bound BtuCD-F, we can integrate the biochemical data into a complete transport cycle that is in agreement with all available structural evidence.

RESULTS

Wild type and mutant BtuCD have similar affinity for BtuF in detergent. To determine the structure of BtuCD bound to AMPPNP, two mutations in the BtuD subunit (E159Q and N162C) were used. The same mutations were previously exploited in the structure determination of the AMPPNP-bound BtuCD-F complex, allowing the closed sandwich conformation of the nucleotide-binding domains (BtuD) to be stabilized and the residual ATPase rate to be dramatically reduced[7]. To confirm that the mutations introduced into $BtuCD_{EQNC}$ have not drastically perturbed the ability of the protein to react to nucleotide and interact with BtuF, we performed *in vitro* binding studies, using fluorescein-labeled BtuF (referred to as "$BtuF_{fluo}$"). $BtuF_{fluo}$ was generated by introducing a cysteine residue (Q145C) at a position distant from the transporter-binding interface, to minimize the effects of labeling on BtuF-BtuCD interaction (Supplementary Fig. 1).

We first used an equilibrium binding technique, microscale thermophoresis (MST), to assess the ability of detergent-solubilized (LDAO) wt BtuCD and $BtuCD_{EQNC}$ to interact with BtuF (Fig. 1). MST allows measurements of equilibrium protein-protein interaction in homogeneous mixtures, without separating the interacting species[9]. The thermophoretic mobility of $BtuF_{fluo}$ was determined as described in "Methods"; changes in its thermophoretic behaviour in the presence of increasing transporter concentrations were used to determine dissociation constants. Both wt BtuCD and $BtuCD_{EQNC}$ showed a strong affinity for $BtuF_{fluo}$, with K_d values in the nanomolar range. Notably, the presence of AMPPNP did not significantly alter the apparent affinities (Fig. 1a-b). The specificity of the interaction was confirmed using non-labeled BtuF as a binding competitor (Supplementary Fig. 2).

To compare the obtained results with those of a non-equilibrium technique, we used sedimentation velocity analytical ultracentrifugation with fluorescence detection[10]. The analysis was performed under similar conditions as the above MST experiments. The concentration of BtuCD was varied, whereas that of $BtuF_{fluo}$ was kept constant, and samples were analysed in the presence or absence of AMPPNP. The mixtures were allowed to equilibrate and were subjected to analytical ultracentrifugation (Fig. 1e-f). In detergent solution, $BtuF_{fluo}$ by itself migrated as a single species of ~0.8S. In the presence of increasing transporter concentrations, a separate species migrating at an

apparent sedimentation coefficient of ~3.5S was observed. As shown in Fig. 1e, $BtuF_{fluo}$ bound detergent-solubilized wild-type BtuCD with high affinity (apparent K_d in the nanomolar range). Addition of AMPPNP appeared to reduce the strength of this interaction. Similar observations were made with $BtuCD_{EQNC}$ (Fig. 1f).

Structure of $BtuCD_{EQNC}$ bound to AMPPNP reveals an outward-facing conformation. To determine the effect of nucleotide binding on the conformation of BtuCD, we crystallized $BtuCD_{EQNC}$ in complex with AMPPNP, but in the absence of BtuF. After extensive screening, crystals belonging to space group *C2* were obtained. A complete dataset was obtained by combining crystallographic data collected from three distinct crystals and multiple positions on each crystal. The X-ray dataset was anisotropic with data ranging from 2.8-3.7Å (Supplementary Table 1). The phase problem was solved by molecular replacement using the BtuCD ensemble from the previously determined structure of $BtuCD_{EQNC}$-F (PDB ID: 4FI3)[7]. Conformational differences to $BtuCD_{EQNC}$-F were evident in the initial maps, and iterative model building and refinement was used to obtain a refined structure. The structure of AMPPNP-bound $BtuCD_{EQNC}$ (Fig. 2a, Supplementary Fig. 3-5) revealed the expected closed sandwich dimer of the BtuD subunits, with two AMPPNP/Mg^{2+} pairs bound at the ATP-binding sites at the domain interface (Supplementary Fig. 4-5). Similar arrangements were observed in $BtuCD_{EQNC}$-F/AMPPNP (PDB ID: 4FI3)[7] and in ATP-bound structures of serveral other ABC transporters. As expected, the coupling helices of the BtuC subunits are ~9.4Å closer in $BtuCD_{EQNC}$ compared to the apo-structures of BtuCD and BtuCD-F (pdb files 1L7V and 2QI9). However, critical differences to the structure of AMPPNP-bound $BtuCD_{EQNC}$-F (PDB ID: 4FI3) were evident in the transmembrane BtuC subunits, most prominently at the periplasmic side of the transporter: Unlike the occluded conformation of AMPPNP-bound $BtuCD_{EQNC}$-F, $BtuCD_{EQNC}$ adopts an outward-open conformation reminiscent of apo-BtuCD. The periplasmic gate of BtuCD is formed by the end of transmembrane helix 5, helix 5', and the loop connecting the two helices. The observed opening results in the formation of a deep pocket at the interface of the BtuC dimer, accessible from the periplasmic side of the membrane (Fig. 2a-c).

In stark contrast to the apo-BtuCD structure[6], the cytoplasmic side of the central transport cavity is not closed by residues of cytoplasmic gate I (beginning of

transmembrane helix 5), but by the cytoplasmic gate II (Fig. 3). With respect to the gate positions, the structure of $BtuCD_{EQNC}$ is therefore a hybrid between apo-BtuCD (similar at periplasmic side) and $BtuCD_{EQNC}$ -F (similar at cytoplasmic side). It is evident from the structure and consistent with biochemical experiments with BtuCD-F[7] and MolBC (HI1470/71)[11] that the closure of cytoplasmic gate II is a direct consequence of nucleotide binding. The structure of $BtuCD_{EQNC}$ represents the first description of a type II ABC importer bound to an ATP analogue, primed for docking of substrate-loaded periplasmic binding protein.

ATP enhances the interaction of BtuF with lipid-reconstituted BtuCD. Because the interaction of BtuF with BtuCD may be influenced by the lipidic environment, we reconstituted BtuCD in proteoliposomes and performed binding assays using $BtuF_{fluo}$ to quantitate the amount of bound binding protein. Compared to empty proteoliposomes, entrapped AMPPNP caused a slight increase in the liposome-bound $BtuF_{fluo}$ fraction. In contrast, entrapped ATP caused a ~2-fold increase in $BtuF_{fluo}$ binding. To ensure that the transporter had sustained access to ATP despite ongoing ATP hydrolysis, an ATP regeneration system was enclosed in the proteoliposome lumen. In all cases, bound $BtuF_{fluo}$ could readily be displaced by unlabeled BtuF (Fig. 4a). Importantly, despite a molar excess of BtuCD in the proteoliposomes, only a fraction of total $BtuF_{fluo}$ was bound within the incubation time of the reaction. In the presence of vitamin B12, the fraction of $BtuF_{fluo}$ bound to the transporter was reduced (Fig. 4b). However, $BtuF_{fluo}$ binding was observed even in the presence of a 100-fold excess of vitamin B12 over binding protein when ATP was present in the proteoliposome lumen.

To obtain an independent assessment of nucleotide effects on BtuCD-BtuF interaction in lipids, we reconstituted BtuCD into nanodiscs (using scaffold protein MSP1-E3D1). Nanodisc-reconstituted BtuCD was incubated with $BtuF_{fluo}$ and the mixtures were analyzed by size exclusion chromatography. In the absence of nucleotide, the SEC profiles revealed incomplete BtuCD-F_{fluo} complex formation, with a significant portion of $BtuF_{fluo}$ remaining unbound (Fig. 5c). Incubation of the transporter/$BtuF_{fluo}$ mixture with ATP caused a sizeable increase in the fraction of full complex (Fig. 5d). Given that size exclusion chromatography is a non-equilibrium technique, the amount of BtuCD-F complex largely depends on the dissociation rate of BtuF, and no K_d values can be

determined from this experiment. Nevertheless, the observed differences in complex formation confirm that ATP enhances the BtuCD-BtuF complex when the transporter is in a lipid bilayer environment.

Using MST experiments we confirmed that the affinity of BtuCD for $BtuF_{fluo}$ is in the micromolar range, regardless of the presence of ATP (i.e. almost 3 orders of magnitude higher than in detergent; Supplemetary Fig. 7). Because a plateau could not be reached within the studied concentration range, accurate K_d values could not be determined.

DISCUSSION

Given that the cytoplasmic concentration of ATP in live cells is in the millimolar range, visualizing the ATP-bound state of BtuCD was essential to formulating a complete B12 transport mechanism. Because BtuCD tends to hydrolyze ATP even when two inhibiting mutations are introduced ("EQNC"), AMPPNP was used for co-crystallization with $BtuCD_{EQNC}$. The essential question was whether the observed structure accurately reflected the conformation of wild type BtuCD with bound ATP. Multiple observations are in favor of this notion: First, the observed closed sandwich dimer of the BtuD subunits with trapped AMPPNP has a similar conformation compared to other ATP-bound ABC transporter (or NBD) structures. Second, our equilibrium and non-equilibrium BtuF binding studies confirmed indistinguishable affinity of BtuF and detergent-solubilized BtuCD or $BtuCD_{EQNC}$. Third, the closing of the cytoplasmic gate II and the simultaneous opening of cytoplasmic gate I (and TM10) were observed by EPR spectroscopy of BtuCD in the presence of ATP or AMPPNP in detergent and in lipid bilayers[12], in full agreement with our crystal structure. This suggests that neither the E159Q nor the N162C mutation resulted in trapping the transporter in a non-physiological conformation. Fourth, EPR spectroscopy revealed very minor changes in the conformation of the periplasmic gate when ATP is added to BtuCD[13], which is in support of our observed, outward-open hybrid conformation.

Using our new $BtuCD_{EQNC}$/AMPPNP structure alone, we were unable to reconcile the contradictory proposed roles of nucleotide binding that have transpired from recently published studies of type II ABC importers. On the one hand, our own structural and biochemical investigations suggested that nucleotide is essential for delivering vitamin B12 to BtuCD as well as for vitamin B12 translocation[7,14]. On the other hand, evidence obtained using surface plasmon resonance suggested that ATP binding and hydrolysis may only be required to lower the affinity of BtuF for BtuCD, prompting complex dissociation and resetting of the system, and not for the actual B12 transport step. This was based on extremely high affinities, determined by surface plasmon resonance, between detergent-solubilized BtuCD and BtuF (K_d of $\sim 10^{-13}$ M^{-1} in the absence of ATP). Such high affinity posed a serious barrier in a transport cycle[8].

We therefore studied the interaction of BtuCD and BtuF both in detergent solution and in lipidic environment, and we find much lower affinities compared to the ones

determined by SPR. Moreover, we find an opposite effect of ATP binding from the one reported[8], leading us to distinctly different mechanistic conclusions. Using MST analysis, we find dissociation constants of BtuF from BtuCD in the range of tens of nanomolar rather than sub-picomolar. Importantly, the presence of nucleotide had very little effect on the affinities. It is notable that a seemingly weaker affinity in the presence of ATP was observed when a non-equilibrium method (AUC) was used to study BtuF-BtuCD binding. While the observed trend matches the one reported for SPR studies[8], we conclude that such studies may suffer from bias and may reflect the physiologically relevant behavior of the transporter only to a limited extent.

The functional characteristics of BtuCD in detergent differ from those of lipid-reconstituted transporter. This includes the rate of ATPase activity and the stimulation of ATPase by BtuF[14]. In addition, recent EPR spectroscopic studies suggested that while many structural features of BtuCD (or BtuCD-F) as observed in crystal structures match EPR findings of lipid-reconstituted transporter, the conformational transitions in detergent can vary significantly from those observed in lipid bilayers[12,13]. We therefore investigated the interaction of BtuCD with BtuF in two distinct lipid environments, proteoliposomes and nanodiscs. Not only are the apparent affinities approximately three orders of magnitude lower (K_d values in the micromolar range), but there is a clear increase of affinity when ATP is bound. This is distinct from all observations in detergent solution. We conclude that the periplasmic binding protein BtuF does not require an ATP “trigger” to be released from its cognate transporter BtuCD. Rather, ATP promotes docking of B12-loaded BtuF and thus accelerates transport.

The above considerations allowed us to formulate a complete transport mechanism for BtuCD-catalyzed B12 transport, as illustrated in Fig. 6. This mechanism may serve as a model of other type II ABC importers. Key aspects of the mechanism are the following:

1. ATP-triggered closure of the BtuD dimer closes the distance between the coupling helices, a conserved transmission mechanism in canonical ABC transporters that was first observed in the ABC multidrug exporter structure Sav1866. However, the movement of coupling helices of BtuCD results in the closing of cytoplasmic gate II and simultaneous opening of cytoplasmic gate I. Given that other types of ABC transporters don't have two cytoplasmic gates, this mechanistic aspect is unique to type II ABC importers.

2. The periplasmic gate does not respond to ATP binding and hydrolysis, but only closes when BtuF is attached to the external face of the transporter, whether ATP is bound to the BtuD subunits or not.

3. BtuCD does not have a high affinity substrate pocket in the transmembrane domain, but a hydrophobic, low-affinity chamber that contains trapped B12 when BtuCD-F is in the ATP-bound state.

4. Distinct roles are assigned to ATP binding and ATP hydrolysis: While ATP binding promotes B12-BtuF docking and the transfer of B12 into the central, intramembrane "teflon chamber", ATP hydrolysis and in particular the release of the hydrolysis products causes cytoplasmic gates to open, releasing B12 into the cytoplasm.

A productive cycle of B12 transport starts with ATP-bound BtuCD (state 1), which is based on the AMPPNP-bound $BtuCD_{EQNC}$ structure reported here. The significance of this outward-facing state is confirmed by our results showing that ATP supports stronger interaction between transporter and periplasmic binding protein. Docking of B12-bound BtuF to BtuCD leads to state 2 (PDB ID: 4FI3), a transient complex that harbors the transported substrate within a central cavity ("teflon chamber"). State 2 is an occluded conformation. To reach state 3, hydrolysis of ATP and release of Pi/ADP disrupts the closed sandwich dimer conformation of the BtuD subunits. The coupling helices and cytoplasmic gates II are pulled open, leading to the formation of a transient, inward-facing transporter conformation, allowing B12 release into the cytoplasm. This is the only state for which no direct structural information is available in BtuCD. However, the homologous Hi1470/71 transporter was structurally characterized in an inward-facing state, allowing a model of inward-facing BtuCD-F to be generated and validate by chemical cross-linking of engineered cysteine disulfide cross-linking[7]. The inward-facing conformation of BtuCD-F is probably short-lived, relaxing into state 4 as soon as B12 is released. It is unclear at this time if B12 release occurs via a peristaltic mechanism (i.e. the sides of the BtuC-formed cavity exerting force/pressure on B12) or simply by diffusion. State 4 is asymmetric, but the observed asymmetry in the cytoplasmic gates 1 is not connected to that of BtuF, because we have determined crystals structures of both asymmetric conformers (PDB ID: 2QI9 and 4DBL). The asymmetric "occluded" state is very stable in detergent solution and does not contain any cavity of sufficient size to harbor B12. Thus this state may prevent the back-reaction or non-specific transport of

solutes through the translocation pathway. From state 4, there are two possible ways. Depending on the concentration of B12-bound BtuF in the periplasm, dissociation of BtuF may lead to state 5 (pdb 1L7V). However, a short-cut can be imagined that bypasses state 1. State 1 is reached from state 4 by dissociation of BtuF and re-arrangement of the cytoplasmic gates I to reach a symmetric, outward-facing conformation. Given the high intra-cellular levels of ATP, state 5 probably rapidly converts to state 1, with the cytoplasmic gates I and II switching positions at the center of the transporter. *In vitro*, states 5 and "2-like" are readily formed, and it cannot be excluded that they also occur i*n vivo*[6,15]. The “futile” transitions involving these transporter conformations, namely those between states 4 and 2-like, as well as states 1 and 5, reflect futile ATPase activity (ATP hydrolysis without transport), an inherent inefficiency of the transport machinery that is consistent with published observations[14]. It is notable that most purified ABC transporters show futile ATPase activity *in vitro*, and for the yeast transporter Pdr5 this activity was demonstrated to be present *in vivo*. Futile ATP hydrolysis makes it close to impossible to make a defintive statement about the stoichiometry of ATP hydrolysis to substrate transport. For one well-coupled system, the OpuA system from *Lactococcus lactis*, a stoichiometry of two molecules of ATP hydrolysed per transported substrate was determined[16]. We assume that BtuCD, having two symmetrical and canonical ATPase sites, also hydrolyzes two ATP molecules during each productive transport cycle.

BtuCD is part of a high-affinity uptake process in *E. coli*. The high affinity (nanomolar K_d) and specificity for B12 can be exclusively attributed to the binding protein BtuF. Upon docking of BtuF to BtuCD, the high-affinity B12 pocket is both distorted (separate motions of the two BtuF lobes as required by interactions with the external loops of BtuC) and occupied by the residues of the periplasmic gate of BtuC. The interaction of BtuF with BtuCD is temporarily strengthened by ATP binding to BtuD, although the structural basis of this subtle regulation is currently not understood. The observation that the affinity of BtuF to apo-BtuCD is "only" in the micromolar range in lipid bilayers is reminiscent of the function of other ABC transporter systems including the maltose transporter (type I ABC transporter[17]), in which the periplasmic maltose binding protein stimulates the ATPase activity of the membrane-embedded counterpart, $MalFGK_2$, when present at micromolar concentrations[18]. Similarly, ABC exporters including lipid flippase MsbA (K_d for lipid A ~5.5 μM[19]), major facilitators such as lactose permease LacY (K_d for

galactose ~50 mM[20]), sodium-dependent solute transporters such as the dopamine transporter DAT (K_i for dopamine ~1.5 μM[21]), small multidrug transporters EmrE (K_m for methyl viologen transport ~250 μM[22]) and others exhibit medium-to-low affinities for their substrates. This prevents clogging of the transport machinery and ensures efficient turnover. The mechanism of type II ABC importer function presented here complies with these requirements for effective substrate translocation.

METHODS

Protein expression and purification. BtuCD and $BtuCD_{EQNC}$ complexes were expressed and purified by Ni-NTA affinity chromatography, as described previously[7], in a final buffer of the following composition: 20 mM Tris (pH7.5), 500 mM NaCl, 0.5 mM EDTA, 0.1% LDAO. For crystallization, the $BtuCD_{EQNC}$ with and without 10xHis tag were used. The 10xHis-tagged $BtuCD_{EQNC}$ was oxidized with $CuCl_2$ (for C162-C162 disulphide bond formation) immediately upon elution from Ni-NTA column In case of non-tagged $BtuCD_{EQNC}$ complex, 3C protease cleavage step was performed prior to oxidation.

Expression and purification of BtuF and $BtuF_{Q145C}$ followed established procedures[23]. $BtuF_{Q145C}$ was labeled with fluorescein-maleimide overnight at 4°C prior to preparative size-exclusion chromatography step using a Superdex 200 10/300 GL column, yielding the final $BtuF_{fluo}$ preparation. Stocks of $BtuF_{fluo}$ were split into aliquots, flash-frozen in liquid nitrogen and stored at -80 °C until the day of experiment.

Membrane scaffold protein for nanodisc reconstitution, MSP1-E3D1[24], was expressed in BL21(DE3)Gold cells using a commercially available vector (Addgene) as described previously[24], and purified by NiNTA affinity chromatography. The 8xHis tag was removed by TEV protease cleavage. Aliquots of MSP1-E3D1 stock were flash frozen in liquid nitrogen until the day of reconstitution.

Proteoliposome reconstitution. Procedure for reconstitution of BtuCD into proteoliposomes followed that described previously[7]. In brief, a mixture of purified BtuCD and lipids was incubated at room temperature for 90 min; detergent was step-wise removed overnight using BioBeads (Biorad) at room temperature and at 4 °C.

Nanodisc reconstitution. Purified BtuCD complex in LDAO was mixed with purified MSP1-E3D1 and lipids (*E. coli* polar lipids and phosphatidylcholine, 3:1, solubilized in 4% Triton X-100), at final concentrations of 12 μM, 72 μM and 2.5 mM; the concentration of lipid mixture was estimated based on molecular weights of the major lipid components. Concentration of Triton X-100 was adjusted to 1%. Following 30 min incubation at room temperature, the BioBeads were added in several steps to the mixture: 15 min at 22 °C (0.1 g BioBeads per 1 ml protein/lipid mixture), 16h at 4 °C (0.5 g Biobeads/1ml mixture), 2h at 4 °C (0.5 g Biobeads/1ml mixture), 15 min at 22 °C (0.2 g Biobeads/1ml mixture). To isolate the nanodiscs containing only BtuCD, after detergent

removal the samples were further purified by Ni-NTA (using 10xHis tag present in BtuC N-terminus) and gel filtration. For isolation of nanodiscs containing lipids only (reconstituted in the absence of BtuCD), the Ni-NTA step prior to gel filtration was omitted.

Centrifugation-based BtuF binding assays. ATP regeneration system was introduced into the lumen of the proteoliposomes by four freeze-thaw cycles, followed by sonication. BtuF binding was initiated by adding fluorescein-labeled BtuF to the BtuCD proteoliposomes and 10 min incubation at room temperature (22 °C), in 20 mM Tris (pH 7.5), 200 mM NaCl, 0.5 mM EDTA, 5 mM $MgCl_2$, 1% BSA. After 10 min centrifugation at 4 °C using a bench-top centrifuge (16900g), supernatants were carefully removed, leaving the proteoliposome pellets intact. Pellets were resuspended in 0.5% Triton X-100 and fluorescence associated with the proteoliposomes was measured using a fluorescence plate reader (ex. 485/20 nm, em. 528/20 nm, sensitivity 50-75). For experiments with vitamin B12, pellets were resuspended in 0.5% SDS to avoid fluorescein quenching by vitamin B12 associated with BtuF.

Size-exclusion chromatography of nanodisc-reconstituted samples. Nanodiscs with or without incorporated BtuCD (2-4 μM final) were mixed with $BtuF_{fluo}$ (0.5-1 μM final) and/or ATP (1 mM) in a buffer of following composition: 20 mM Tris (pH 7.5), 200 mM NaCl, 0.5 mM EDTA, 5 mM $MgCl_2$. The mixtures were incubated for 20 min at 4C and injected into Superdex 200 5/150 GL column (with 100 μl fractions collected) or Superdex 200 10/300 GL column (with 240 μl fracions collected). Elution was monitored online using absorbance at 280 nm; fractions were analyzed using fluorescence plate reader.

Analytical ultracentrifugation. Analytical centrifugation was performed using ProteomeLab XL-I analytical centrifuge (Beckman) equipped with fluorescence detection system (AVIV Biomedical). Sedimentation velocity experiments were performed using $BtuF_{fluo}$ and BtuCD or $BtuCD_{EQNC}$ in 50 mM Tris (pH 7.5), 500 mM NaCl, 0.5 mM EDTA, 5 mM $MgCl_2$ ± 2 mM AMPPNP, at 10 °C, at 50000 rpm, as described previously[10]. A mixture of $BtuF_{fluo}$ (10 nM) and a range of concentrations of BtuCD or $BtuCD_{EQNC}$ (10-1000 nM) were used. Buffer density and viscosity were calculated using the SEDNTERP software. Sedimentation coefficient traces were calculated using the SEDFIT software[25].

Microscale thermophoresis. Microscale thermophoresis was performed using Monolith NT.115 (NanoTemper Technologies), following the manufacturer's instructions. In brief, protein samples of interest (a range of concentrations of BtuCD in LDAO or nanodiscs and $BtuF_{fluo}$ at 25 nM concentration) were mixed in the presence or abence of 1 mM ATP, incubated at 10 °C for 20 min. Capillaries filled with the sample mixtures were introduced into the microscale thermophoresis instrument and the measurements were performed using the following settings: for $BtuF_{fluo}$ vs BtuCD in LDAO LED power 20%, MST power 80%; for $BtuF_{fluo}$ vs BtuCD in nanodiscs LED power 80%, MST power 80%. The results were analysed using NanoTemper software to determine K_d values. GraphPad Prism 5 was used to plot the data and perform statistical analysis (one-way ANOVA).

Protein crystallization and data collection. Purified tag-free $BtuCD_{EQNC}$ in 20 mM Tris, 500 mM NaCl, 0.5 mM EDTA, 5 mM $MgCl_2$, 2 mM AMPPNP, was crystallized by vapour diffusion in a sitting drop set up, using 24-well Cryschem plates (Hampton Research). Freshly purified protein was concentrated to 16-20 mg/ml and mixed with a solution containing 100 mM ADA (pH 6.9), 1.2 M NaCl, 14-18% PEG2000 MME, 1:1 in a total volume of 3.2-4 µl. Crystals grew at 10 °C and reached final size within a week. Crystals were cryo-protected by step-wise addition of a harvesting solution containing increasing concentrations of PEG2000MME (final concentration of 30-32%), and flash frozen in liquid nitrogen. Crystallographic data collection was performed using the microfocus diffractometer and the PX beamline (Swiss Light Source, Villigen, Switzerland).

Crystallographic data processing and model building. Data processing was performed using HKL2000[26]. A merged dataset was obtained by scaling three individually collected datasets using Denzo and Scalepack. All datasets were anisotropic, with resolution extending to 2.8 Å, 3.0 Å and 3.7 Å in a, b and c direction, respectively. Final scaled dataset was submitted to the diffraction anisotropy server for ellipsoidal truncation and anisotropic scaling[27]. Structure was determined by molecular replacement using Phenix[28], with $BtuCD_{EQNC}$ ensemble from a previous PDB entry (PDB ID: 4FI3)[7] as a search model. Model building was performed in Coot[29] and refinement was performed in Phenix. Crystallographic data summary is shown in Supplementary Table 1.

FIGURE LEGENDS

Figure 1: Biophysical characterization of $BtuF_{fluo}$ binding to BtuCD/$BtuCD_{EQNC}$ in detergent. (a-b) Schematic illustrating BtuCD (in **b** - $BtuCD_{EQNC}$) in detergent micelles (orange cones) with $BtuF_{fluo}$ in the presence or absence of AMPPNP, as used in the experiments in **c-f**. The yellow line connecting the two BtuD subunits in $BtuCD_{EQNC}$ represents the disulfide cross-link. **(c-d)** Microscale thermophoresis data of $BtuF_{fluo}$ binding to BtuCD (**c**) or $BtuCD_{EQNC}$ (**d**). The observed affinities are indistinguishable in all four cases. (**d**; here and in **f** $BtuCD_{EQNC}$ is labeled as "EQNC"). Normalized fluorescence of $BtuF_{fluo}$ (Fnorm) is plotted against transporter concentration. The calculated K_d ± SEM values are as follows: "BtuCD", 4.3 ± 5 nM (n = 5); "BtuCD + AMPPNP", 0.85 ± 2.5 nM (n = 4); "EQNC", 6.8 ± 6.6 nM (n = 7); "EQNC + AMPPNP", 1.3 ± 3.8 nM (n = 7). The values were not significantly different, judged by one-way ANOVA ($P > 0.05$). **(e)** Sedimentation velocity analytical ultracentrifugation, performed as described in "Methods" using mixtures of $BtuF_{fluo}$ and BtuCD in the absence or presence of AMPPNP (apparent K_d of 7.3 ± 5.9 and 311 ± 425, respectively). (**f**). Experiments as in **e**, with mixtures of $BtuF_{fluo}$ and $BtuCD_{EQNC}$ in the absence or presence of AMPPNP (apparent K_d of 16.4 ± 8.2 and 260 ± 113, respectively). In the presence of AMPPNP, the interaction appears weakened because separation during a sedimentation velocity experiment is irreversible. Results shown represent ratio of the observed fraction with sedimentation coefficient of ~3.5S (bound) to that with sedimentation coefficient of ~0.8S, plotted against transporter concentration (each data point represents mean ± SEM, n = 2).

Figure 2: Structure of AMPPNP-bound $BtuCD_{EQNC}$ in an outward-facing conformation. (a) Side views of the structure of $BtuCD_{EQNC}$ with two molecules of AMPPNP bound. BtuC subunits are colored marine and blue, BtuD subunits are colored forest and pale green; AMPPNP molecules are depicted at the interface of the BtuD dimer. Two molecules of LDAO per BtuC monomer, modeled based on well-resolved electron density features, are colored in green. **(b-c)** Comparison of apo-BtuCD ("BtuCD"; PDB ID: 1L7V) and $BtuCD_{EQNC}$/AMPPNP ("EQNC/AMPPNP") illustrating movement of the coupling helices (indicated) but similarly open periplasmic gates. Arrows indicate the direction of the conformational rearrangements.

Figure 3: AMPPNP-induced switch of cytoplasmic gates. (a) View of apo-BtuCD (PDB ID: 1L7V) from the cytoplasmic side of the membrane; atoms of residues forming the cytoplasmic gates I and II are shown as spheres, as indicated. The seal is maintained by mutual contacts between residues T142-S143 of the cytoplasmic gate I (residues S141-S143 are highlighted). **(b)** Equivalent view of $BtuCD_{EQNC}$/AMPPNP complex from the cytoplasmic side of the membrane shows that the translocation pathway is sealed by cytoplasmic gate II residues (highlighted residues: N83-L85).

Figure 4: $BtuF_{fluo}$ binding to proteoliposome-reconstituted BtuCD (a) Schematic representation of experiment shown in **b**, wherein the effect of luminal AMPPNP or ATP (resupplied by ATP regeneration system "ARS") on the binding of $BtuF_{fluo}$ was tested. $BtuF_{fluo}$, but not unlabeled BtuF, is indicated by a green hexagon. **(b)** Quantitation of bound $BtuF_{fluo}$ is shown under various conditions. The content of the proteoliposome lumen is indicated below the horizontal axis, the concentration of competing, unlabeled BtuF is indicated. Data shown are mean ± SEM, n = 4. **(c-d)** Experiments were performed as in **b**, but in the absence of unlabeled BtuF; instead, all reactions were performed in the absence or presence of 100-fold molar excess of vitamin B12 over BtuF (2.5 μM), as illustrated in **c.** Data shown are mean ± SEM, n = 3; data for "25 nM $BtuF_{fluo}$" are independent from those shown in **b**.

Figure 5: Binding of $BtuF_{fluo}$ to nanodisc-reconstituted BtuCD. (a-d) Size exclusion chromatography of $BtuF_{fluo}$ alone (**a**), mixed with empty nanodiscs (MSP1-E3D1) (**b**), BtuCD-containing nanodiscs (**c**), or BtuCD-containing nanodiscs and ATP (**d**). Schematics to the right of each panel illustrate the experimental setup. The protein mixtures were incubated at 4°C for 20 min prior to injection onto a Superdex 200 10/300 GL column. Eluted fractions (200 μl each) were collected and the amount of $BtuF_{fluo}$ in each fraction was determined using a fluorescence plate reader. Each experiment was reproduced 2-4 times in total, using either a Superdex 200 10/300 GL or a Superdex 200 5/150 GL columns.

Figure 6: Mechanism of BtuCD-F-catalyzed B12 transport cycle. Grey cylinder cartoons illustrate structures of BtuCD, BtuF, or BtuCD-F, circled numbers indicate states as discussed in text. Yellow ball-and-sticks represent nucleotides, red ball-and-sticks depict cobalamin. Thick blue lines depict transmembrane helices 5 in each BtuC subunit, forming the periplasmic gates and the cytoplasmic gates I. Purple brackets depict the cytoplasmic gates II in each BtuC subunit. For details and discussion of the mechanism see text.

FIGURES

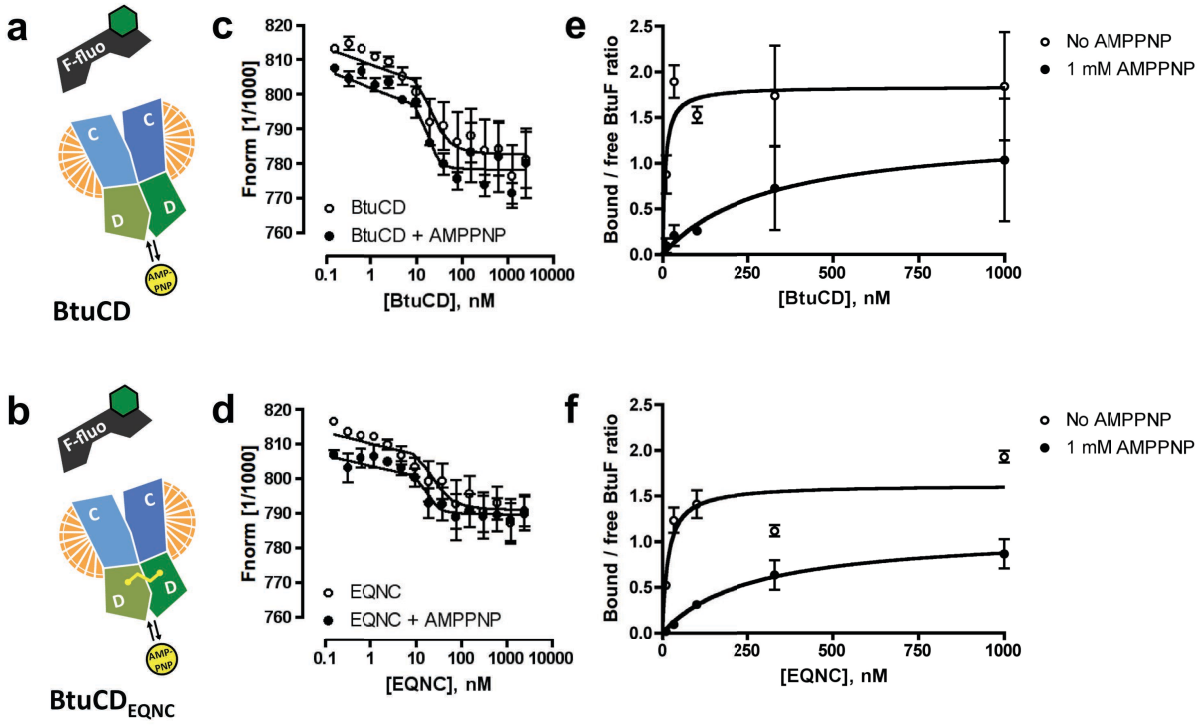

Figure 1: Biophysical characterization of $BtuF_{fluo}$ binding to BtuCD/$BtuCD_{EQNC}$ in detergent. (a-b) Schematic illustrating BtuCD (in **b** - $BtuCD_{EQNC}$) in detergent micelles (orange cones) with $BtuF_{fluo}$ in the presence or absence of AMPPNP, as used in the experiments in **c-f**. The yellow line connecting the two BtuD subunits in $BtuCD_{EQNC}$ represents the disulfide cross-link. **(c-d)** Microscale thermophoresis data of $BtuF_{fluo}$ binding to BtuCD (**c**) or $BtuCD_{EQNC}$ (**d**). The observed affinities are indistinguishable in all four cases. (**d**; here and in **f** $BtuCD_{EQNC}$ is labeled as "EQNC"). Normalized fluorescence of $BtuF_{fluo}$ (Fnorm) is plotted against transporter concentration. The calculated K_d ± SEM values are as follows: "BtuCD", 4.3 ± 5 nM (n = 5); "BtuCD + AMPPNP", 0.85 ± 2.5 nM (n = 4); "EQNC", 6.8 ± 6.6 nM (n = 7); "EQNC + AMPPNP", 1.3 ± 3.8 nM (n = 7). The values were not significantly different, judged by one-way ANOVA ($P > 0.05$). **(e)** Sedimentation velocity analytical ultracentrifugation, performed as described in "Methods" using mixtures of $BtuF_{fluo}$ and BtuCD in the absence or presence of AMPPNP (apparent K_d of 7.3 ± 5.9 and 311 ± 425, respectively). (**f**). Experiments as in **e**, with mixtures of $BtuF_{fluo}$ and $BtuCD_{EQNC}$ in the absence or presence of AMPPNP (apparent K_d of 16.4 ± 8.2 and 260

± 113, respectively). In the presence of AMPPNP, the interaction appears weakened because separation during a sedimentation velocity experiment is irreversible. Results shown represent ratio of the observed fraction with sedimentation coefficient of ~3.5S (bound) to that with sedimentation coefficient of ~0.8S, plotted against transporter concentration (each data point represents mean ± SEM, n = 2).

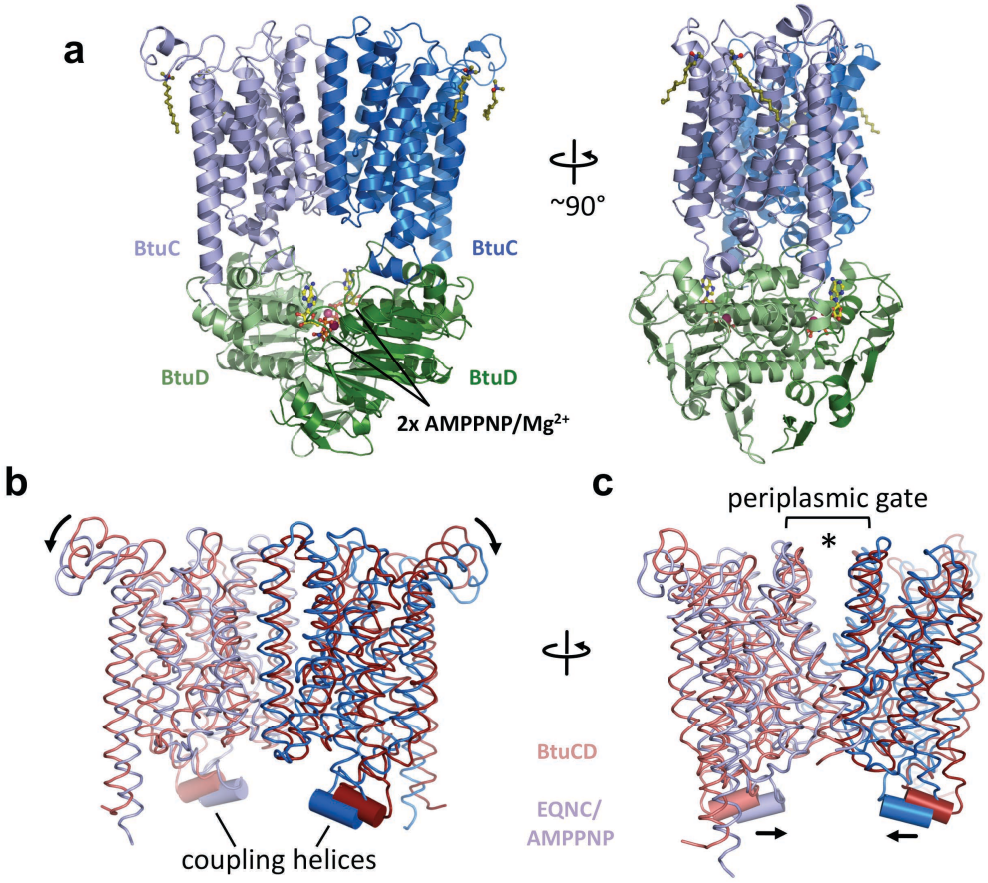

Figure 2: Structure of AMPPNP-bound $BtuCD_{EQNC}$ in an outward-facing conformation. (a) Side views of the structure of $BtuCD_{EQNC}$ with two molecules of AMPPNP bound. BtuC subunits are colored marine and blue, BtuD subunits are colored forest and pale green; AMPPNP molecules are depicted at the interface of the BtuD dimer. Two molecules of LDAO per BtuC monomer, modeled based on well-resolved electron density features, are colored in green. **(b-c)** Comparison of apo-BtuCD ("BtuCD"; PDB ID: 1L7V) and $BtuCD_{EQNC}$/AMPPNP ("EQNC/AMPPNP") illustrating movement of the coupling helices (indicated) but similarly open periplasmic gates. Arrows indicate the direction of the conformational rearrangements.

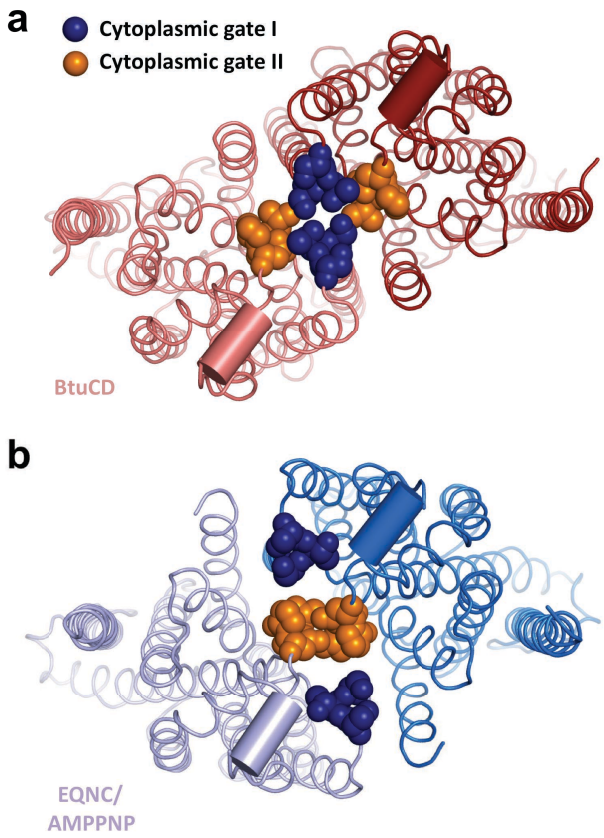

Figure 3: AMPPNP-induced switch of cytoplasmic gates. (a) View of apo-BtuCD (PDB ID: 1L7V) from the cytoplasmic side of the membrane; atoms of residues forming the cytoplasmic gates I and II are shown as spheres, as indicated. The seal is maintained by mutual contacts between residues T142-S143 of the cytoplasmic gate I (residues S141-S143 are highlighted). **(b)** Equivalent view of $BtuCD_{EQNC}$/AMPPNP complex from the cytoplasmic side of the membrane shows that the translocation pathway is sealed by cytoplasmic gate II residues (highlighted residues: N83-L85).

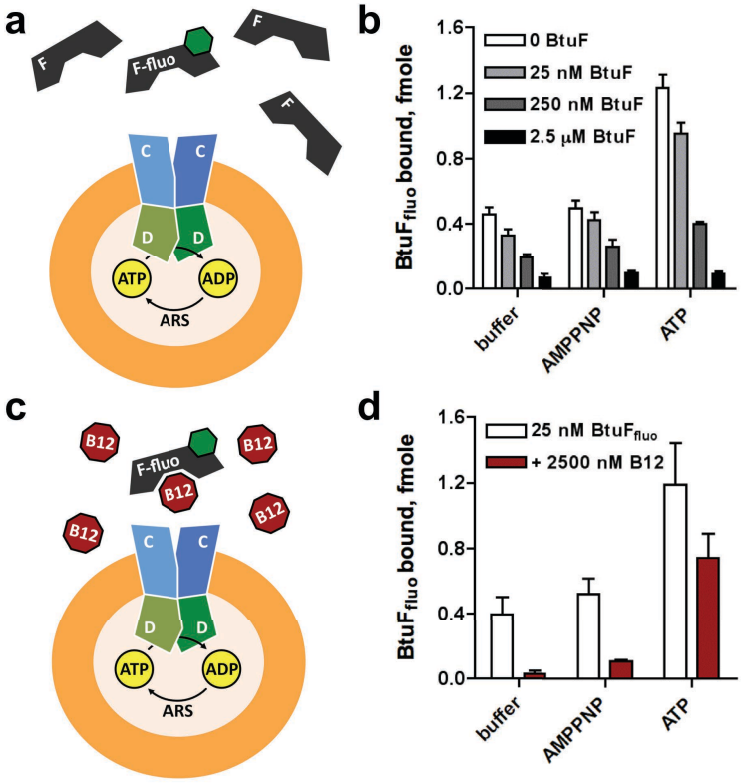

Figure 4: BtuF$_{fluo}$ binding to proteoliposome-reconstituted BtuCD (a) Schematic representation of experiment shown in **b**, wherein the effect of luminal AMPPNP or ATP (resupplied by ATP regeneration system "ARS") on the binding of BtuF$_{fluo}$ was tested. BtuF$_{fluo}$, but not unlabeled BtuF, is indicated by a green hexagon. **(b)** Quantitation of bound BtuF$_{fluo}$ is shown under various conditions. The content of the proteoliposome lumen is indicated below the horizontal axis, the concentration of competing, unlabeled BtuF is indicated. Data shown are mean ± SEM, n = 4. **(c-d)** Experiments were performed as in **b**, but in the absence of unlabeled BtuF; instead, all reactions were performed in the absence or presence of 100-fold molar excess of vitamin B12 over BtuF (2.5 μM), as illustrated in **c.** Data shown are mean ± SEM, n = 3; data for "25 nM BtuF$_{fluo}$" are independent from those shown in **b**.

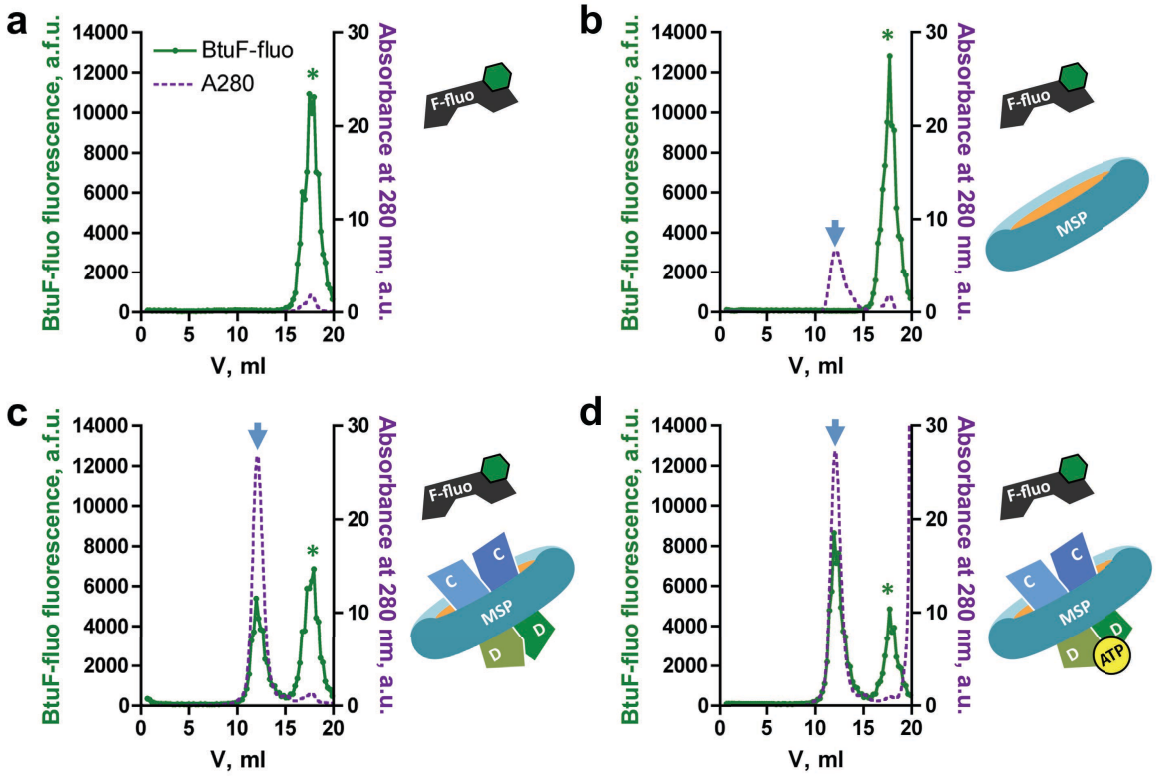

Figure 5: Binding of $BtuF_{fluo}$ to nanodisc-reconstituted BtuCD. (a-d) Size exclusion chromatography of $BtuF_{fluo}$ alone (**a**), mixed with empty nanodiscs (MSP1-E3D1) (**b**), BtuCD-containing nanodiscs (**c**), or BtuCD-containing nanodiscs and ATP (**d**). Schematics to the right of each panel illustrate the experimental setup. The protein mixtures were incubated at 4°C for 20 min prior to injection onto a Superdex 200 10/300 GL column. Eluted fractions (200 µl each) were collected and the amount of $BtuF_{fluo}$ in each fraction was determined using a fluorescence plate reader. Each experiment was reproduced 2-4 times in total, using either a Superdex 200 10/300 GL or a Superdex 200 5/150 GL columns.

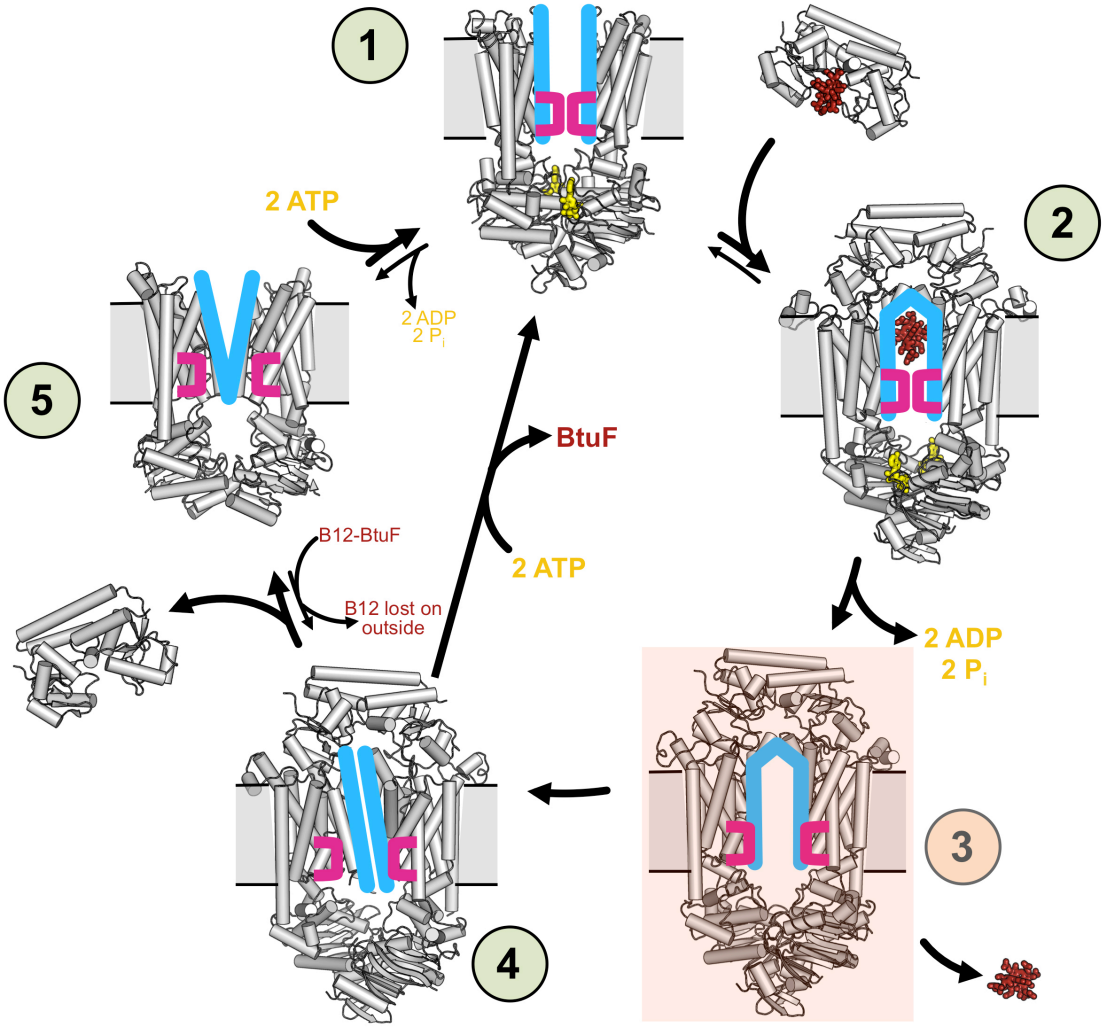

Figure 6: Mechanism of BtuCD-F-catalyzed B12 transport cycle. Grey cylinder cartoons illustrate structures of BtuCD, BtuF, or BtuCD-F, circled numbers indicate states as discussed in text. Yellow ball-and-sticks represent nucleotides, red ball-and-sticks depict cobalamin. Thick blue lines depict transmembrane helices 5 in each BtuC subunit, forming the periplasmic gates and the cytoplasmic gates I. Purple brackets depict the cytoplasmic gates II in each BtuC subunit. For details and discussion of the mechanism see text.

REFERENCES

1. Rees, D.C., Johnson, E. & Lewinson, O. ABC transporters: the power to change. *Nat Rev Mol Cell Biol* **10**, 218-27 (2009).
2. Oldham, M.L., Davidson, A.L. & Chen, J. Structural insights into ABC transporter mechanism. *Curr Opin Struct Biol* **18**, 726-33 (2008).
3. Klein, J.S. & Lewinson, O. Bacterial ATP-driven transporters of transition metals: physiological roles, mechanisms of action, and roles in bacterial virulence. *Metallomics* **3**, 1098-108 (2011).
4. Bassford, P.J., Jr., Bradbeer, C., Kadner, R.J. & Schnaitman, C.A. Transport of vitamin B12 in tonB mutants of Escherichia coli. *J Bacteriol* **128**, 242-7 (1976).
5. Locher, K.P. & Borths, E. ABC transporter architecture and mechanism: implications from the crystal structures of BtuCD and BtuF. *FEBS Lett* **564**, 264-8 (2004).
6. Locher, K.P., Lee, A.T. & Rees, D.C. The E. coli BtuCD structure: a framework for ABC transporter architecture and mechanism. *Science* **296**, 1091-8 (2002).
7. Korkhov, V.M., Mireku, S.A. & Locher, K.P. Structure of AMP-PNP-bound vitamin B12 transporter BtuCD-F. *Nature* **490**, 367-72 (2012).
8. Lewinson, O., Lee, A.T., Locher, K.P. & Rees, D.C. A distinct mechanism for the ABC transporter BtuCD-BtuF revealed by the dynamics of complex formation. *Nat Struct Mol Biol* **17**, 332-8 (2010).
9. Jerabek-Willemsen, M., Wienken, C.J., Braun, D., Baaske, P. & Duhr, S. Molecular interaction studies using microscale thermophoresis. *Assay Drug Dev Technol* **9**, 342-53 (2011).
10. Brandt, T., Petrovich, M., Joerger, A.C. & Veprintsev, D.B. Conservation of DNA-binding specificity and oligomerisation properties within the p53 family. *BMC Genomics* **10**, 628 (2009).
11. Rice, A.J. et al. EPR spectroscopy of MolB2C2-a reveals mechanism of transport for a bacterial type II molybdate importer. *J Biol Chem* **288**, 21228-35 (2013).
12. Joseph, B., Korkhov, V.M., Yulikov, M., Jeschke, G. & Bordignon, E. Conformational cycle of the vitamin B12 ABC importer in liposomes detected by DEER. *J Biol Chem* (2013).
13. Joseph, B., Jeschke, G., Goetz, B.A., Locher, K.P. & Bordignon, E. Transmembrane gate movements in the type II ATP-binding cassette (ABC) importer BtuCD-F during nucleotide cycle. *J Biol Chem* **286**, 41008-17 (2011).
14. Borths, E.L., Poolman, B., Hvorup, R.N., Locher, K.P. & Rees, D.C. In vitro functional characterization of BtuCD-F, the Escherichia coli ABC transporter for vitamin B12 uptake. *Biochemistry* **44**, 16301-9 (2005).
15. Woo, J.S., Zeltina, A., Goetz, B.A. & Locher, K.P. X-ray structure of the Yersinia pestis heme transporter HmuUV. *Nat Struct Mol Biol* **19**, 1310-5 (2012).
16. Patzlaff, J.S., van der Heide, T. & Poolman, B. The ATP/substrate stoichiometry of the ATP-binding cassette (ABC) transporter OpuA. *J Biol Chem* **278**, 29546-51 (2003).
17. Chen, J. Molecular mechanism of the Escherichia coli maltose transporter. *Curr Opin Struct Biol* **23**, 492-8 (2013).
18. Gould, A.D., Telmer, P.G. & Shilton, B.H. Stimulation of the maltose transporter ATPase by unliganded maltose binding protein. *Biochemistry* **48**, 8051-61 (2009).
19. Siarheyeva, A. & Sharom, F.J. The ABC transporter MsbA interacts with lipid A and amphipathic drugs at different sites. *Biochem J* **419**, 317-28 (2009).

20. Sugihara, J., Smirnova, I., Kasho, V. & Kaback, H.R. Sugar recognition by CscB and LacY. *Biochemistry* **50**, 11009-14 (2011).
21. Kitayama, S. et al. Dopamine transporter site-directed mutations differentially alter substrate transport and cocaine binding. *Proc Natl Acad Sci U S A* **89**, 7782-5 (1992).
22. Yerushalmi, H., Lebendiker, M. & Schuldiner, S. EmrE, an Escherichia coli 12-kDa multidrug transporter, exchanges toxic cations and H+ and is soluble in organic solvents. *J Biol Chem* **270**, 6856-63 (1995).
23. Korkhov, V.M., Mireku, S.A., Hvorup, R.N. & Locher, K.P. Asymmetric states of vitamin B(1)(2) transporter BtuCD are not discriminated by its cognate substrate binding protein BtuF. *FEBS Lett* **586**, 972-6 (2012).
24. Ritchie, T.K. et al. Chapter 11 - Reconstitution of membrane proteins in phospholipid bilayer nanodiscs. *Methods Enzymol* **464**, 211-31 (2009).
25. Schuck, P., Perugini, M.A., Gonzales, N.R., Howlett, G.J. & Schubert, D. Size-distribution analysis of proteins by analytical ultracentrifugation: strategies and application to model systems. *Biophys J* **82**, 1096-111 (2002).
26. Otwinowski, Z. & Minor, W. Processing of X-ray diffraction data collected in oscillation mode. *Macromolecular Crystallography, Pt A* **276**, 307-326 (1997).
27. Strong, M. et al. Toward the structural genomics of complexes: crystal structure of a PE/PPE protein complex from Mycobacterium tuberculosis. *Proc Natl Acad Sci U S A* **103**, 8060-5 (2006).
28. Adams, P.D. et al. PHENIX: a comprehensive Python-based system for macromolecular structure solution. *Acta Crystallogr D Biol Crystallogr* **66**, 213-21 (2010).
29. Emsley, P., Lohkamp, B., Scott, W.G. & Cowtan, K. Features and development of Coot. *Acta Crystallogr D Biol Crystallogr* **66**, 486-501 (2010).